

Tailoring GaAs, InAs, and InGaAs Nanowires for Optoelectronic Device Applications

Hannah J. Joyce, *Student Member, IEEE*, Qiang Gao, *Member, IEEE*, Jennifer Wong-Leung, Yong Kim, H. Hoe Tan, *Senior Member, IEEE*, and Chennupati Jagadish, *Fellow, IEEE*

Abstract—GaAs, InAs, and InGaAs nanowires each exhibit significant potential to drive new applications in electronic and optoelectronic devices. Nevertheless, the development of these devices depends on our ability to fabricate these nanowires with tight control over critical properties, such as nanowire morphology, orientation, crystal structure, and chemical composition. Although GaAs and InAs are related material systems, GaAs and InAs nanowires exhibit very different growth behaviors. An understanding of these growth behaviors is imperative if high-quality ternary InGaAs nanowires are to be realized. This report examines GaAs, InAs, and InGaAs nanowires, and how their growth may be tailored to achieve desirable material properties. GaAs and InAs nanowire growth are compared, with a view toward the growth of high-quality InGaAs nanowires with device-accessible properties.

Index Terms—III–V nanowires, electron microscopy, semiconductor nanowires.

I. INTRODUCTION

SEMICONDUCTOR nanowires have been heralded as the future nanobuilding blocks for electronic and optoelectronic devices. Indeed, a broad range of nanowire-based devices have already been developed, including nanowire solar cells [1], waveguides [2], photodetectors [3], [4], light-emitting diodes [5], [6], lasers [7], [8], single-photon sources [9], resonant-tunneling diodes [10], single-electron transistors and memory devices [11]–[13], field-emission sources [14], field-effect transistors for ultrahigh density logic and memory devices [15]–[18], integrated photonic circuits [19], [20], and highly sensitive biological and chemical sensors [21].

GaAs and InAs nanowires are especially promising for optoelectronic device applications due to the superior electrical

and optical properties of their constituent III–V materials. These materials feature a direct bandgap and high electron mobility. The GaAs material system is currently of great importance in the electronics and optoelectronics industries, and accordingly, GaAs nanowires are prime candidates for electrically and optically active nanowire devices. InAs features very high electron mobility at room temperature which makes InAs nanowires particularly promising for use in high-speed electronic devices [15], [22]. InAs also exhibits surface Fermi level pinning in the conduction band [23], which permits facile formation of low-resistance ohmic contacts [15]. As a testament to the utility of GaAs and InAs nanowires, a large proportion of the aforementioned devices were created using GaAs or InAs nanowires and associated heterostructures [4]–[18].

Ternary $\text{In}_x\text{Ga}_{1-x}\text{As}$ nanowires are expected to drive high-power and high-frequency electronics, long wavelength optical transmission, and integrated photonics, as the $\text{In}_x\text{Ga}_{1-x}\text{As}$ material system is already used extensively for these purposes. In addition, the bandgap of $\text{In}_x\text{Ga}_{1-x}\text{As}$ can be varied over a large range by changing the In mole fraction x . InGaAs nanowires would enable a greater range of axial and radial heterostructures, and thus, broaden the application range of nanowires. Hereafter, we simply refer to $\text{In}_x\text{Ga}_{1-x}\text{As}$ as InGaAs to describe the full range of alloys between $x = 0$ and 1.

Despite the obvious importance of InGaAs nanowires, there have been only a handful of reports on their growth [24]–[28] and even fewer on InGaAs nanowire-based devices [29]. InGaAs nanowire growth is known to be complicated by the different growth behaviors of the In and Ga elements comprising the nanowire [24]. In most growth systems, the In and Ga species differ significantly in their decomposition efficiencies, solubility, diffusion properties, and incorporation efficiencies [24]. Consequently, there are major difficulties in controlling the composition and uniformity of InGaAs nanowires, which severely hamper the development of InGaAs nanowire-based devices.

To enable future fabrication of high-quality InGaAs nanowires, it is important to first understand the similarities and differences between GaAs and InAs nanowire growth. In addition, GaAs and InAs nanowires are important in their own right, and comparison of the growth systems gives considerable insight into the growth mechanisms. Thus, the impressive potential of GaAs, InAs, and InGaAs nanowires for future devices motivates detailed investigation of their growth.

This report examines Au nanoparticle-assisted growth of GaAs, InAs, and InGaAs nanowires by metal–organic chemical vapor deposition (MOCVD). Arguably, this fabrication process is the most promising and most widespread growth technique for

Manuscript received July 1, 2010; revised August 19, 2010; accepted September 2, 2010. Date of publication October 28, 2010; date of current version August 5, 2011. This work was supported by the Australian Research Council.

H. J. Joyce was with the Department of Electronic Materials Engineering, Research School of Physics and Engineering, Australian National University, Canberra ACT 0200, Australia. She is now with the Department of Physics, University of Oxford, Oxford, U.K. (e-mail: h.joyce1@physics.ox.ac.uk).

Q. Gao, J. Wong-Leung, H. H. Tan, and C. Jagadish are with the Department of Electronic Materials Engineering, Research School of Physics and Engineering, Australian National University, Canberra ACT 0200, Australia (e-mail: gao109@physics.anu.edu.au; jwl109@physics.anu.edu.au; hoe109@physics.anu.edu.au; cxj109@physics.anu.edu.au).

Y. Kim is with the Department of Physics, College of Natural Sciences, Dong-A University, Sahagu, Busan 604-714, Korea (e-mail: yongkim@dau.ac.kr).

Digital Object Identifier 10.1109/JSTQE.2010.2077621

III–V nanowires: it achieves epitaxial III–V nanowires via a Au nanoparticle-assisted vapor–liquid–solid (VLS) or vapor–solid–solid process [30], [31]. MOCVD is the method of choice for many applications in electronics and optoelectronics [32]–[34]. It is a highly accurate and flexible growth technique, and offers a number of parameters that can be controlled independently to achieve the desired properties in the grown sample. These parameters include growth temperature, V/III ratio, and growth rate. The V/III ratio is the ratio of group V to group III growth precursor flow rates, and it is widely acknowledged as a crucial factor in III–V growth [35]. The growth rate is controlled by scaling the flow rates of both the group III and group V precursors, which we refer to as “absolute” precursor flow rate.

We investigate how these growth parameters affect nanowire growth, and how they can be tailored to achieve desirable nanowire properties. We highlight the differences between GaAs and InAs nanowire growth, with a view toward fabricating high-quality InGaAs nanowires.

II. NANOWIRE GROWTH

All nanowires presented were grown by MOCVD using Au nanoparticles to drive nanowire growth. Trimethylgallium (TMGa) and trimethylindium (TMI) were the precursors for group III elements Ga and In, respectively. The group V element As was provided by arsine (AsH₃). GaAs nanowires and InGaAs nanowires were grown on semiinsulating GaAs(111)B substrates. InAs nanowires were grown on undoped InAs(111)B substrates. Before growth, substrates were treated with 0.1% poly-L-lysine (PLL) solution for 60 s, and rinsed in DI water to remove excess PLL, and dried with N₂. Then, a 50 μL droplet of colloidal Au nanoparticles (50 nm diameter) in aqueous solution was applied to each substrate surface and left for 20 s, after which the excess was rinsed away with DI water and substrates were dried with N₂. The negatively charged colloidal nanoparticles adhere to the positively charged PLL layer, as described in previous reports [24], [36].

Nanowires, seeded by these nanoparticles, were grown by horizontal flow MOCVD at a pressure of 100 mbar and a total gas flow rate of 15 000 standard cubic centimeters per minute (sccm) using H₂ carrier gas. Prior to growth initiation, the substrate was annealed in situ at 600 °C under AsH₃ ambient to desorb surface contaminants. After cooling to the desired temperature, the group III precursor (TMG and/or TMI) was introduced to initiate nanowire growth. The standard, or control, group III flow rate was III₀ = 1.2 × 10⁻⁵ mol/min (0.27 sccm). The standard group V flow rate was V₀ = 5.4 × 10⁻⁴ mol/min (12 sccm), which gives a standard V/III ratio of 46.

GaAs nanowires were grown by either a single-temperature or a two-temperature procedure. The single-temperature procedure involved 15 min of growth at a constant temperature T_g between 350 and 550 °C. For the two-temperature procedure, growth was initiated with a 1 min “nucleation” step at the nucleation temperature T_n of 450 °C. The temperature was rapidly ramped down to the subsequent “growth” temperature T_g between 325 and 425 °C. The total growth time t was 15 min, and the cooling time was typically 1.5–6.5 min.

InAs nanowires were grown by a single-temperature procedure at a constant temperature T_g between 375 and 550 °C. The standard growth time t was 30 min.

For GaAs and InAs nanowires, the effects of V/III ratio and absolute precursor flow rate were studied as follows. To study V/III ratio, the group III flow rate was maintained at III₀, and AsH₃ flow rates were chosen between 1/4, 1/2, 1, and 2 times V₀ to achieve V/III ratios varying in binary orders of magnitude, of 12, 23, 46, and 93. To study the effect of absolute precursor flow rate, III₀ and V₀ were scaled by factors of 1/4, 1/2, 1, 2, 4, and 8. Groups III and V flows were scaled equally so that the V/III ratio remained constant at 46. The growth time t was scaled inversely with group III flow, to achieve nanowires of reasonable height of approximately 1–5 μm across all samples.

InGaAs nanowires were grown by either a single-temperature or a two-temperature procedure. The single-temperature procedure involved 30 min of growth at a constant temperature T_g between 375 and 450 °C. For the two-temperature procedure, growth was initiated with a 1 min “nucleation” step at the nucleation temperature T_n of 450 °C. The temperature was rapidly ramped down to the subsequent “growth” temperature T_g between 375 and 425 °C. Total growth time was 30 min, including the nucleation and cooling steps, and typical cooling time was between 1.5 and 4 min. Source flows of TMGa, TMI, and AsH₃ were 1.2 × 10⁻⁵ mol/min (0.27 sccm), 3.9 × 10⁻⁶ mol/min (0.087 sccm), and 5.4 × 10⁻⁵ mol/min (12 sccm), respectively, which represents a 25% vapor In composition and 75 % vapor Ga composition ($x_{v,\text{In}} = 0.25$ and $x_{v,\text{Ga}} = 0.75$).

III. CHARACTERIZATION AND GROWTH METRICS

Field-emission scanning electron microscopy (FESEM) was employed to identify the general morphology of the nanowires, including growth direction, height, diameter, tapering, and facet planes. Transmission electron microscopy (TEM) was employed to accurately resolve smaller scale structure, such as variations in nanowire width. For TEM images, nanowires were mechanically transferred to holey carbon-coated copper grids. Nanowires were imaged along the $\langle 1\bar{1}0 \rangle$ zone axis, perpendicular to the nanowire growth direction.

Axial growth is the term describing the [1 1 1]B-oriented, elongating nanowire growth. There are three contributions to axial growth: 1) reaction species, which directly impinge on the nanoparticle; 2) reaction species, which are adsorbed on the nanowire sidewalls and diffuse up the nanowire sidewalls to the nanoparticle; and 3) reaction species, which are adsorbed on the substrate and diffuse up the nanowire sidewalls to the nanoparticle. The diffusing species may be the group III precursor itself (e.g., TMGa), or one of its decomposition products, such as the monomethyl product (e.g., monomethylgallium, MMGa), or the elemental group III adatom (e.g., Ga). Radial growth describes the lateral growth on the nanowire sidewalls. This receives contributions from pathways 2) and 3). Axial and radial growths are illustrated in Fig. 1. Growth may also occur on the substrate.

The axial growth rate R_{axial} was estimated by measuring nanowire heights L from FESEM images and dividing L by the growth time t . The axial growth rate was only calculated

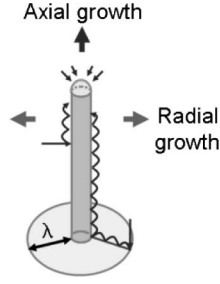


Fig. 1. Schematic illustration of axial and radial nanowire growth. It shows the direct impingement of precursor species on the nanoparticle at the nanowire tip, and the diffusion of adsorbed species from the substrate and along the nanowire sidewalls. It also shows the diffusion length on the substrate λ .

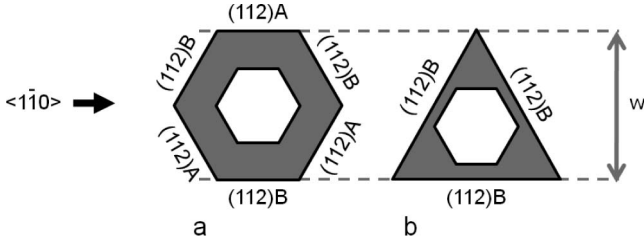


Fig. 2. Schematic illustration of possible nanowire cross sections, and the nanowire width w , as measured from a $\langle 1\bar{1}0 \rangle$ viewing angle.

for straight $[1\bar{1}1]B$ -oriented nanowires. At least 20 nanowires were examined for each data point, and the measurements were averaged to give the plotted data.

Note that both GaAs and InAs generally exhibit $\{1\bar{1}2\}$ side facets, as illustrated in Fig. 2. The six $\{1\bar{1}2\}$ side facets are polar, and can be subdivided into three $\{1\bar{1}2\}A$ and three $\{1\bar{1}2\}B$ side facets. Nanowires may feature all six $\{1\bar{1}2\}$ side facets to give a hexagonal cross section, as shown in Fig. 2(a). Under certain conditions, rapid growth occurs on $\{1\bar{1}2\}A$ side facets, which causes the $\{1\bar{1}2\}B$ facets to become elongated [37]–[39]. In this case, the nanowire cross section tends to adopt a more triangular shape, as shown in Fig. 2(b). As illustrated in Fig. 2, an image taken along a $\langle 1\bar{1}0 \rangle$ axis (perpendicular to the substrate cleavage plane) gives an accurate representation of the total radial growth on the two opposite $\{1\bar{1}2\}A$ and $\{1\bar{1}2\}B$ side facets.

For this reason, FESEM images of nanowires tilted to the $\langle 1\bar{1}0 \rangle$ axis were used to measure w , the nanowire width. We define the nanowire “radius” r as half the nanowire width w .

To calculate radial growth, we first calculate the increment in nanowire radius Δr per increment in nanowire length Δl . This is equivalent to the ratio of radial (R_{radial}) to axial (R_{axial}) growth rates, and is known as the tapering parameter

$$\text{Tapering parameter} = \frac{\Delta r}{\Delta l} \approx \frac{R_{\text{radial}}}{R_{\text{axial}}}. \quad (1)$$

Measurements of Δr and Δl were taken from FESEM images at consecutive intervals of approximately $1\ \mu\text{m}$ in length, along each nanowire from the Au nanoparticle–nanowire interface to the base. For each length interval ($\Delta l \approx 1\ \mu\text{m}$), the tapering parameter was determined. This was then averaged for each nanowire. For each sample, measurements of Δr were also taken

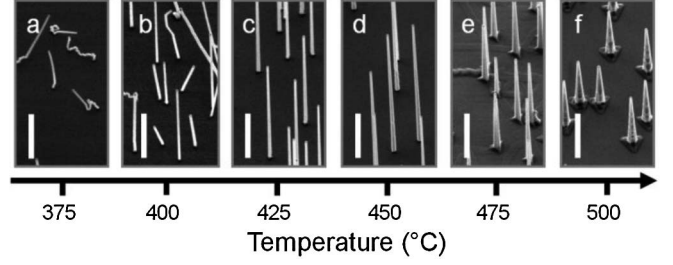


Fig. 3. FESEM images of GaAs nanowires grown by the single-temperature procedure at different temperatures T_g , as indicated. The V/III ratio was 46 and the groups III and V flow rates were III_0 and V_0 for all samples. Scale bars are $1\ \mu\text{m}$. Samples are tilted at 40° .

from TEM images, to confirm the data taken from FESEM images.

The radial growth rate R_{radial} was quantified for each nanowire by multiplying its tapering parameter by its R_{axial} , according to (1). At least 20 nanowires were examined for each data point.

These calculations assume that R_{axial} and R_{radial} are constant over the growth time t . In reality, R_{axial} and R_{radial} can change with t during the early stages of growth [40]. This occurs as a result of contributions 2) and 3): as the nanowire height increases, a lower proportion of substrate- and sidewall-adsorbed species can diffuse the entire distance to the nanowire tip. This effect is discussed in detail in [40]. Our extracted values of R_{axial} and R_{radial} , despite lacking t dependency, still give a reasonable representation of the growth processes.

TEM was also used to identify crystal structures and the presence of twin-phase boundaries and stacking faults. This is important because the crystallographic phase, whether zinc-blende (ZB) or wurtzite (WZ), directly affects the bandgap, electronic, and optical properties of the nanowires. Energy dispersive X-ray spectroscopy (EDS) was used to study the composition of the nanowires.

IV. RESULTS AND ANALYSIS

A. GaAs Nanowires

We first examine GaAs nanowires. Growth temperature has a marked effect on GaAs nanowire properties. Fig. 3 illustrates FESEM images of nanowires grown at different T_g by the conventional single-temperature procedure. When grown at T_g of 410°C and above, nanowires were straight and epitaxially aligned in the vertical $[1\bar{1}1]B$ direction. In contrast, the majority of nanowires grown below 410°C exhibit irregular kinked morphologies.

The two-temperature differs from the single-temperature procedure: it involves a brief high-temperature nucleation step at T_n before prolonged growth at T_g . Unlike the single-temperature procedure, the two-temperature procedure produced straight, vertical $[1\bar{1}1]B$ -oriented nanowires at T_g as low as 350°C [36]. Fig. 4 illustrates FESEM images of nanowires grown at different T_g using the two-temperature procedure.

Adjunct studies using different T_n revealed that the two-temperature procedure is equally effective for T_n between

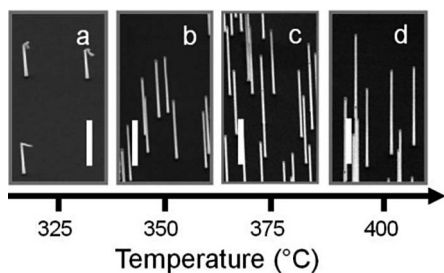


Fig. 4. FESEM images of GaAs nanowires grown by the two-temperature procedure with nucleation temperature T_n of 450 °C and growth temperatures T_g , as indicated. The V/III ratio was 46 and the groups III and V flow rates were III_0 and V_0 , respectively, for all samples. Scale bars are 1 μm . Samples are tilted at 40°.

410 and 500 °C. These results illustrate that to achieve straight [1 1 1]B-oriented nanowires, growth must be initiated at or above a minimum nucleation temperature $T_{n,\text{min}}$ of 410 °C, and thereafter, must be maintained at or above a minimum growth temperature $T_{g,\text{min}}$ of 350 °C. Below $T_{g,\text{min}}$, nanowire growth becomes kinked and irregular. This is apparent in the nanowires of Fig. 4(a), whose lower portions are vertical and [1 1 1]B-oriented and whose upper portions are kinked and irregular. The lower portions grew during the nucleation step and during cooling to T_g , and the kinked upper portions grew below $T_{g,\text{min}}$, at 325 °C.

It is thought that kinking and the success of the two-temperature procedure, are consequences of the physical state of the alloyed Au nanoparticle during growth. This is explained as follows. According to the conventional VLS growth mechanism, the Au nanoparticle forms a eutectic liquid alloy with the reaction species. In the case of GaAs nanowires, Ga is soluble in Au, whereas, As has negligible solubility, so an Au–Ga alloy nanoparticle forms [31], [41]. This liquid alloy drives nanowire growth. If the nanoparticle is solid, however, nanowire growth may be considerably slowed, may cease completely, or may become unstable leading to kinked nanowire morphologies [42], [43]. We believe that kinking occurs in Fig. 3(a) and (b) because the Au nanoparticle is not adequately melted at these low T_g . This is reasonable because these T_g are close to the eutectic point of the Au–Ga system (339.3 °C). Note that the cited T_g are measured by a thermocouple in the reactor, and it gives readings, which are generally a few ten of degrees higher than the true substrate temperature.

The Au–Ga–As ternary phase diagram shows a pseudobinary tie line between Au and GaAs [44]. This tie line indicates that GaAs substrates and Au nanoparticles do not react under AsH_3 overpressure. Therefore, the Au nanoparticle does not alloy with Ga supplied from the GaAs substrate, as discussed in [31]. Instead, the Au–Ga alloy forms only when Ga is supplied as TMGa at growth initiation. Another consideration is melting–solidification hysteresis as observed for Au–Ga nanoparticles in [43]: a higher temperature was observed to melt the nanoparticle, which could then be supercooled and remain liquid until a solidification temperature. In [43], the authors observed a 60 °C difference between melting and solidification temperatures. This is reminiscent of the 60 °C difference we observe

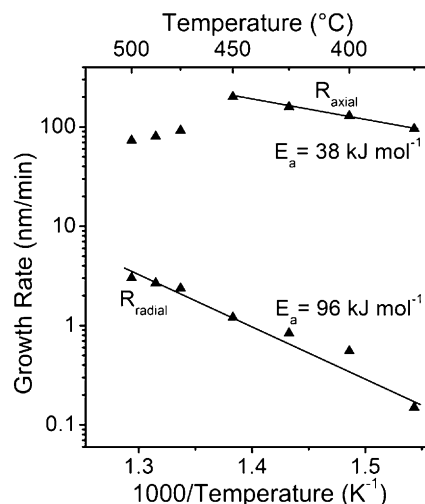


Fig. 5. Temperature dependence of axial and radial growth rates for GaAs nanowires. Abscissa scale is logarithmic. The V/III ratio was 46 and the groups III and V flow rates were III_0 and V_0 , respectively, for all samples.

between $T_{n,\text{min}}$ and $T_{g,\text{min}}$. We infer that the nucleation step of the two-temperature procedure melts the nanoparticle, and the nanoparticle remains liquid when supercooled to the lower T_g . The liquid nanoparticle drives straight, [1 1 1]B-oriented nanowire growth, provided it is melted at a temperature of $T_{n,\text{min}}$ or above, and maintained in a liquid state at a temperature of $T_{g,\text{min}}$ and above.

The temperature dependence of R_{axial} and R_{radial} is plotted in Fig. 5. To produce this plot, only single-temperature-grown nanowires were examined because the brief high-temperature nucleation and cooling steps alter the growth kinetics of the two-temperature grown nanowires, albeit marginally. Only straight [1 1 1]B-oriented nanowires were examined. The plot extends down to 375 °C, because a small proportion of straight [1 1 1]B-aligned nanowires could be found even for single-temperature samples grown at 375 °C. The apparent Arrhenius activation energy E_a is extracted for each plot in Fig. 5.

Such plots help ascertain the growth pathways and limiting factors. In particular, growth may be kinetically limited, i.e., limited by thermally activated chemical reactions such as TMGa and AsH_3 decomposition. Alternatively, growth may be mass transport limited, i.e., limited by the supply of group III species to the growth interface. In the mass transport limited case, surface reactions are faster than the diffusion of the limiting species to the growth interface.

The radial growth rate monotonically increases with temperature with an apparent E_a of 96 kJ/mol. This value is close to that determined by Reep and Ghandhi for planar growth in the low temperature, kinetically limited growth regime [45]. We can infer that radial growth is kinetically limited. Figs. 3 and 4 illustrate that tapering increases as growth temperature is increased, due to the significant radial growth occurring at higher temperatures.

Axial growth exhibits a more complex dependency on growth temperature. Between 375 and 450 °C, R_{axial} increases with temperature with an apparent E_a of 38 kJ mol⁻¹. This E_a is significantly lower than that calculated for R_{radial} . We cannot yet

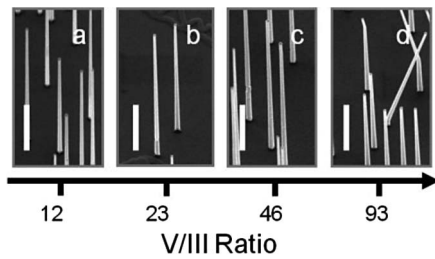


Fig. 6. FESEM images of GaAs nanowires grown at the indicated V/III ratios. The growth temperature was 450 °C and the group III flow was III_0 for all samples. Scale bars are 1 μm . Samples are tilted at 40°.

exclude the possibility that the nanoparticle behaves as a chemical catalyst and lowers the activation energy for axial growth. Interestingly, a recent study proposed that the nanoparticle catalyzes the decomposition of TMGa to a mobile MMGa species, which then diffuses considerable distances and enhances the growth of adjacent nanowires [46]. Another study suggested that Au nanoparticles catalyze AsH_3 pyrolysis [47]. However, a number of other studies have concluded that the Au nanoparticle is not a chemical catalyst; instead it enhances axial GaAs nanowire growth simply by enhancing the transport of material to the nanoparticle–nanowire growth interface [48]–[50].

Above 450 °C, R_{axial} decreases. This occurs due to the onset of significant radial and substrate growth, which compete with axial growth for adsorbed diffusing Ga species [36]. In other words, the mass transport of Ga species limits axial growth above 450 °C. Note that R_{axial} is lower at 500 °C than at 375 °C. This indicates that diffusing Ga species contribute to axial growth even at low temperatures.

This temperature dependence suggests that in the temperature range examined, axial GaAs nanowire growth lies in the transition region between kinetically limited and mass transport limited growth regimes, with mass transport effects becoming more dominant at higher temperatures. Note that the apparent E_a is higher than that reported by Reep and Ghandhi for mass transport-limited planar GaAs growth, but lower than their reported value for kinetically limited planar GaAs growth [45]. It is likely that our extracted E_a is low, not because of any catalytic effect of the nanoparticle, but because of mass transport effects: competitive radial growth increases with temperature, so that at higher temperatures R_{axial} is lower than predicted by reaction kinetics.

Next, we examine the effects of V/III ratio on GaAs nanowire growth. Fig. 6 shows FESEM images of nanowires grown at various V/III ratios, and Fig. 7 plots R_{axial} and R_{radial} against V/III ratio. As the V/III ratio is increased, there is a very marginal increase in R_{axial} , peaking at a V/III ratio of 46. Typically, mass transport limited growth exhibits no dependency on AsH_3 flow: growth is limited by the diffusion of the less abundant species, TMGa, to the growth interface [45]. In contrast, kinetically controlled growth exhibits a weak positive dependence on AsH_3 flow: AsH_3 species lower the activation energy for GaAs growth [45], [51]. The trend in Fig. 6 lies in between, consistent with R_{axial} being governed by both mass transport and kinetic limitations. R_{radial} exhibits a more significant increase with AsH_3 , because it is kinetically limited.

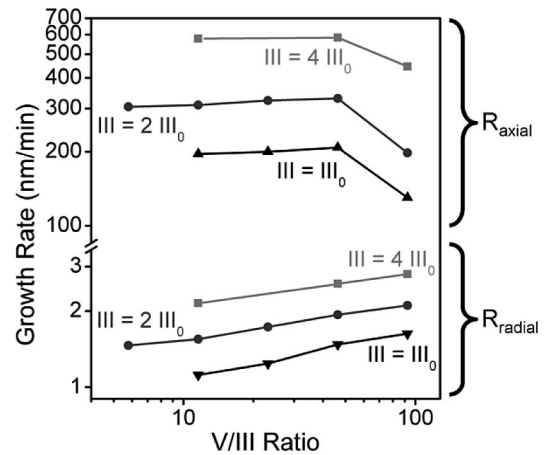


Fig. 7. Axial and radial growth rates of GaAs nanowires for different V/III ratios. Straight lines connect data sets for a constant group III flow rate. All samples were grown at 450 °C. Axes are logarithmic.

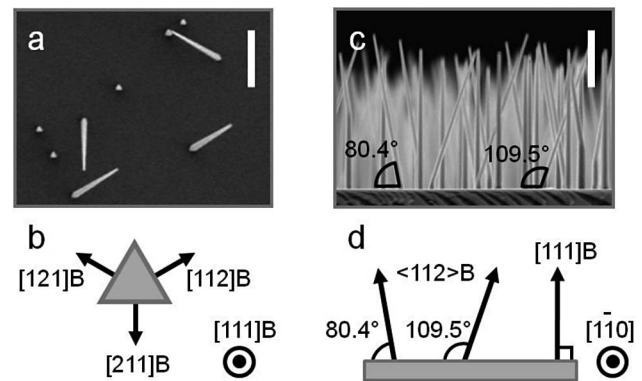


Fig. 8. (a) and (c) FESEM images of nanowires grown at a high V/III ratio of 93 as in Fig. 6(d). (b) and (d) Schematic illustrations of the $\langle 112 \rangle\text{B}$ and $[111]\text{B}$ growth directions. (a) Plan view FESEM image and (b) schematic illustration showing the three $\langle 112 \rangle\text{B}$ and single $[111]\text{B}$ growth directions. (c) View of nanowires along the $\langle 110 \rangle$ direction perpendicular to the $(1\bar{1}0)$ substrate cleavage plane and (d) schematic illustration showing the $\langle 112 \rangle\text{B}$ and $[111]\text{B}$ growth directions as viewed along this $\langle 110 \rangle$ direction. Scale bars are 1 μm .

Beyond a V/III ratio of 46, the axial growth rate drops steeply. This effect cannot be attributed to increased competition from radial growth, because R_{radial} only undergoes a modest increase which is insufficient to account for the drastic reduction in R_{axial} . In addition, beyond a V/III ratio of 46, a proportion of nanowires adopt a non- $[111]\text{B}$ -orientation. Fig. 6(d) and (e), respectively, are tilted and plan view images showing non- $[111]\text{B}$ -oriented nanowires grown at a high V/III ratio of 93. To ascertain the growth direction, FESEM images were taken in plan view [see, e.g., Fig. 8(a)] and along $\langle 1\bar{1}0 \rangle$ directions perpendicular to the $\{1\bar{1}0\}$ substrate cleavage planes [see, e.g., Fig. 8(c)]. Using plan view images [see, e.g., Fig. 8(a)], these growth directions were indexed against the dominant $\{112\}\text{B}$ nanowire side facets and against the $\{1\bar{1}0\}$ substrate cleavage planes. In Fig. 8(c), we observe that the non- $[111]\text{B}$ nanowires grow at angles of 80.4° and 109.5° to the substrate plane. These measurements confirm that the non- $[111]\text{B}$ nanowires grow in three equivalent $\langle 112 \rangle\text{B}$ growth directions. In summary, at high V/III ratios,

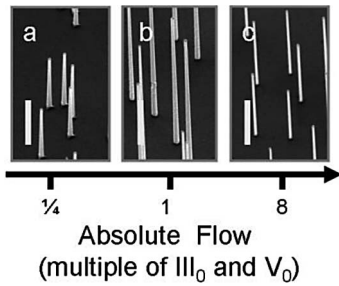


Fig. 9. FESEM images of GaAs nanowires grown at the indicated absolute precursor flow rates. (a) $\frac{1}{4}$ III_0 and $\frac{1}{4}$ V_0 for $t = 60$ min, (b) 1 III_0 and 1 V_0 for $t = 15$ min, and (c) 8 III_0 and 8 V_0 for $t = 112.5$ s. All samples were grown at 450°C with a V/III ratio of 46. Scale bars are $1\ \mu\text{m}$. Samples are tilted at 40° .

nanowires either initiate in and maintain their $[1\ 1\ 1]\text{B}$ growth direction, initiate in and maintain a $\langle 1\ 1\ 2\rangle\text{B}$ direction, or initiate in the $[1\ 1\ 1]\text{B}$ growth direction and later kink to a $\langle 112\rangle\text{B}$ direction.

The simultaneous observations of $\langle 1\ 1\ 2\rangle\text{B}$ growth and growth rate reduction at high V/III ratio suggest that these phenomena are related. In fact, stable As trimers form on the $[1\ 1\ 1]\text{B}$ surface at high V/III ratios, and this surface reconstruction is known to decrease the $[1\ 1\ 1]\text{B}$ growth rate [52]. This surface reconstruction is also thought to make $[1\ 1\ 1]\text{B}$ growth direction less energetically favorable than the $\langle 1\ 1\ 2\rangle\text{B}$ directions [53]. Interestingly, these results suggest that a high V/III ratio can be used to select the $\langle 1\ 1\ 2\rangle\text{B}$ growth direction rather than $[1\ 1\ 1]\text{B}$. This would offer a novel and simple means of creating branched nanowires and 3-D interconnected nanowire networks.

Further analysis of the effects of V/III ratio on GaAs nanowires is given in [53].

The absolute precursor flow rate also had a profound effect on nanowire morphology. Fig. 9 illustrates FESEM images of GaAs nanowires grown at different absolute precursor flow rates with a V/III ratio of 46. Fig. 10 plots R_{axial} and R_{radial} . R_{axial} increases significantly with increasing absolute precursor flow rate, similar to the observations of [50]. A linear increase is expected for mass transport limited growth, whereas a weak sublinear increase is expected for kinetically limited growth. The observed trend for R_{axial} is in between these two cases. In contrast, R_{radial} shows a much weaker dependence on absolute flow rate, consistent with kinetically limited growth [45]. Because R_{axial} increases significantly and R_{radial} increases only marginally, a high absolute flow rate reduces nanowire tapering. This is evidenced by the minimally tapered wires of Fig. 9(c).

We have thus demonstrated that nanowire morphology can be controlled using these growth parameters. Significantly, we found that, GaAs nanowire crystal structure can also be tailored using these growth parameters. Increasing the growth temperature increases the occurrence of twin defects, which effectively leads to a more WZ crystal structure [36], [39]. Increasing the V/III ratio decreases the density of twin defects, which effectively promotes a ZB crystal structure [39], [53]. Using a low growth temperature coupled with a high V/III ratio, we achieved pure ZB nanowires without any twin defects [39]. Conversely, by

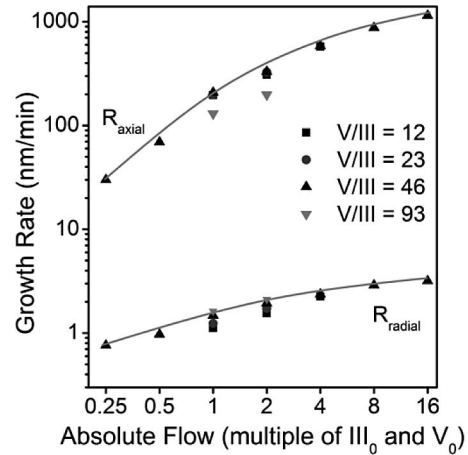


Fig. 10. Axial and radial growth rates of GaAs nanowires for different group III flow rates. All samples were grown at 450°C . The lines are guides for the eye. Axes are logarithmic.

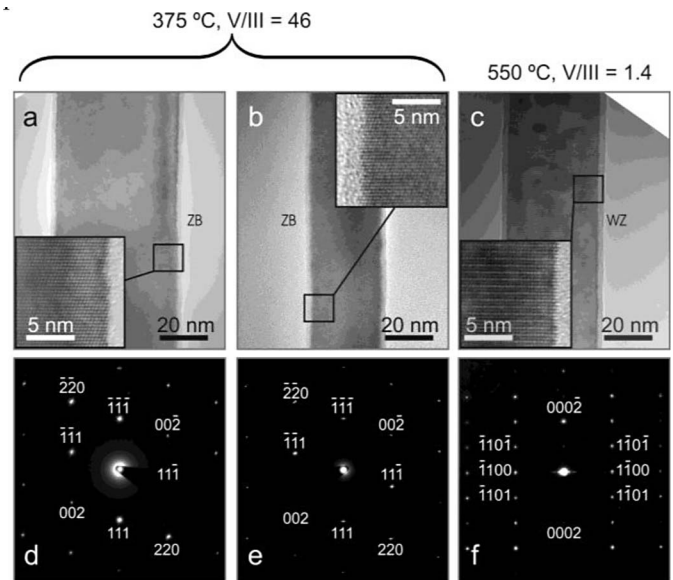


Fig. 11. TEM results for GaAs nanowires. (a)–(c) HRTEM images of pure ZB and pure WZ nanowires and (d)–(f) their respective selected area diffraction patterns. The insets in (a)–(c) show higher magnification images of the pure ZB and WZ nanowires. The nanowires were grown with different nanoparticle sizes of (a) 50, (b) 20, and (c) 30 nm. Reproduced with permission from [39].

coupling a high temperature with a low V/III ratio, we achieved pure WZ nanowires, free of stacking faults [39]. HRTEM images of these pure ZB and pure WZ nanowires are shown in Fig. 11.

In addition, GaAs nanowire optical properties are sensitive to these growth parameters. For these measurements, nanowires were clad in AlGaAs shells to passivate the GaAs surface, as described in [54]. Time-resolved photoluminescence measurements revealed that an increase in V/III ratio significantly reduces the exciton lifetime, probably due to the incorporation of excess As-related defects at high V/III ratios. The defect is most likely the EL2 defect, which is believed to be isolated arsenic antisite defect (As_{Ga}). It creates a deep donor level in GaAs near midgap and acts as an electron trap. Nanowires grown at

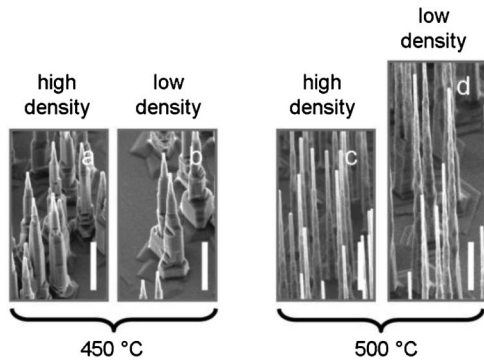


Fig. 12. FESEM images of InAs nanowires grown at (a) and (b) 450 °C and (c) and (d) 500 °C. The areas feature high nanowire density in (a) and (c), and low nanowire density in (b) and (d). The V/III ratio was 46 and the groups III and V flow rates were III₀ and V₀, respectively, for all samples. Scale bars are 1 μm. Samples are tilted at 40°.

a low growth temperature exhibited long, nearly intrinsic excitation lifetimes up to 1 ns [55]. Continuous wave photoluminescence measurements revealed that the donor–acceptor pair peak, which results from carbon acceptor impurities, diminishes for nanowires grown at low temperatures, high V/III ratios, and high absolute precursor flow rates. These conditions, therefore, reduce carbon impurity incorporation [53], [56]. Low-temperature grown nanowires also exhibit higher carrier mobility than those grown at higher temperatures [57].

B. InAs Nanowires

In some respects, InAs nanowire growth behavior parallels that of GaAs nanowires, and in other respects there are major differences. The first major difference is the sensitivity of InAs nanowire growth to the density of nanowires on the substrate. This is clearly exemplified in Fig. 12(c) and (d). In Fig. 12(d), nanowires are more sparsely distributed than in part c. The low-density nanowires of part d are significantly taller and have much wider bases than their high-density counterparts of part c.

This can be explained with reference to the schematic illustration of Fig. 13. In areas of high nanowire density, adjacent nanowires compete for reaction species that are adsorbed on the substrate. In low-density regions, on the other hand, there is minimal competition for diffusing species so the axial growth rate is maximum. The degree of density dependence depends on the diffusion length λ on the (1 1 1)B substrate surface. If λ is long, as in the upper part of Fig. 13, then a significant fraction of axial growth arises from these adsorbed species diffusing from the substrate to the nanoparticle. In this case, density dependence is marked. If λ is short, as in the lower part of Fig. 13, the density dependence is more marginal because nanowires must be very closely spaced to compete for diffusing reaction species. This explains why the nanowires of Fig. 12(a) and (b) do not exhibit such a marked density dependence as those of Fig. 12(c) and (d). The nanowires of Fig. 12(a) and (b) were grown at a lower temperature, which resulted in a shorter diffusion length and consequently a lower density dependence.

This contrasts strongly with GaAs nanowire growth. None of the GaAs nanowires samples exhibited any significant den-

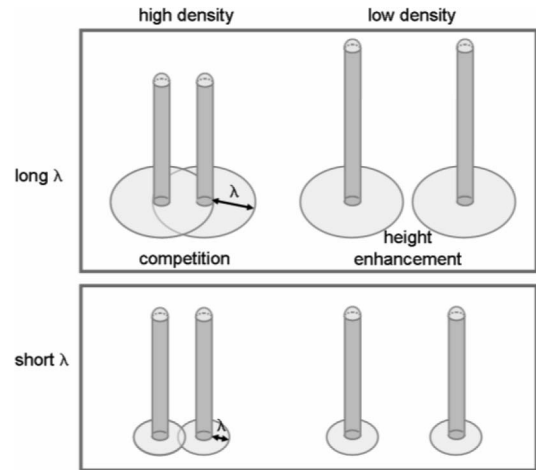


Fig. 13. Schematic illustration of the competition between adjacent nanowires for species adsorbed on the substrate. This illustrates high and low density nanowire regions, and the effects of diffusion length λ . When λ is long, the density dependencies are more significant: significant competition occurs in high-density regions, and whereas significant height enhancement occurs in low-density regions.

sity dependence. Typically, the diffusion length of Ga species is significantly shorter than that of In species, so diffusion of adsorbed species plays a more significant role in InAs nanowire growth [40] than in GaAs nanowire growth.

These density dependences vary with temperature, V/III ratio, and absolute precursor flow rate, because these variables affect the diffusion length. In the following discussion on InAs nanowire growth, only regions of similar nanowire density are compared so that density effects do not obscure the results.

Further insight can be gained by comparing the decomposition and reaction processes of TMGa and TMIIn. Homogeneous decomposition reactions are those which take place in the vapor phase H₂ ambient. TMIIn decomposes homogeneously above 300 °C, and its decomposition increases with temperature until it is completely decomposed at 400 °C [58]. TMGa decomposes homogeneously above 375 °C, and is not completely decomposed until 475 °C [59]. The relatively low homogeneous decomposition temperature of TMIIn compared with TMGa suggests that kinetic limitations will be less significant for InAs nanowire growth.

The aforementioned discussion considers the independent decomposition of each precursor species. It should be noted that when both TMGa (or TMIIn) and AsH₃ are supplied, these precursors generally decompose by reacting with each other. For instance, planar GaAs growth follows the Langmuir–Hinschelwood model, whereby TMGa and AsH₃ adsorb independently on the substrate surface and then react together in a 1:1 ratio to progressively eliminate CH₄ molecules and deposit GaAs [45], [60]. The mechanism of planar InAs growth has not been studied so extensively. It may follow a pathway analogous to GaAs growth. Another possibility is the formation of a gas phase TMIIn:AsH₃ adduct, which adsorbs on the substrate surface and then undergoes decomposition [61].

Comparison of planar GaAs and planar InAs growth gives further insight. Planar GaAs growth is kinetically controlled at

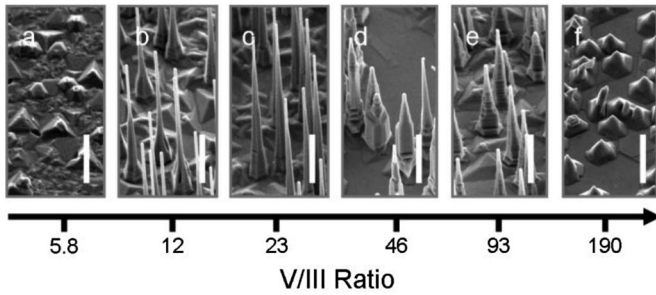


Fig. 14. FESEM images of InAs nanowires grown with different V/III ratios, as indicated. The growth temperature was 450 °C and the group III flow was III_0 for all samples. Scale bars are 1 μm . Samples are tilted at 40°.

low temperatures and is diffusion limited above 600 °C [45]. In contrast, planar InAs growth is kinetically controlled only until 400 °C, and is diffusion limited above this temperature [62]. This suggests, as already inferred from the homogeneous decomposition temperatures, that kinetic limitations may be less significant for InAs nanowire growth than for GaAs nanowire growth.

Compared with GaAs nanowire growth, InAs nanowire growth is confined to a narrower window of growth temperatures, V/III ratios, and absolute precursor flow rates. This will be discussed in the following. A comprehensive quantitative analysis of InAs nanowire growth is presented in [63], and the results discussed here give additional insight into InAs nanowire growth.

First, we examine the effects of V/III ratio with FESEM images shown in Fig. 14 and growth rates plotted in Fig. 15. Nanowires grow only within a finite range of V/III ratios. At the lowest V/III ratios, for example Fig. 14(a), an irregular layer covers the surface, and the Au nanoparticles have failed to nucleate nanowires. Pits in the substrate surface evidence decomposition of the InAs substrate. Nanoparticles have been observed in these pits, suggesting that the Au itself enhances substrate decomposition. This is expected, because compared with GaAs, InAs is more reactive with Au and at a given temperature, requires a higher arsenic overpressure to prevent substrate decomposition [64]. This explains why the V/III window for InAs nanowire growth is narrower than that of GaAs nanowires.

As V/III ratio is increased, there are sufficient As species to promote nanowire growth, therefore, R_{axial} increases sharply. This has also been observed in [63]. R_{radial} also increases, resulting in nanowire tapering.

The axial growth rate reaches a maximum at a V/III ratio of 23, beyond which it decreases. This decrease is possibly because diffusion length diminishes with increasing V/III ratio [65], so that adsorbed In species are less likely to diffuse to the nanowire tip and incorporate into axial growth [66]. The species are more likely to incorporate close to the site of adsorption, either on the nanowire sidewalls or on the substrate [66]. For this reason, R_{radial} continues to increase with V/III ratio.

At the highest V/III ratios, R_{axial} slows considerably, the Au-assisted structures appear island-like rather than nanowire-like, and the short nanostructures often follow $\langle 1\ 1\ 2 \rangle$ directions rather than $[1\ 1\ 1]\text{B}$ directions. This parallels the growth be-

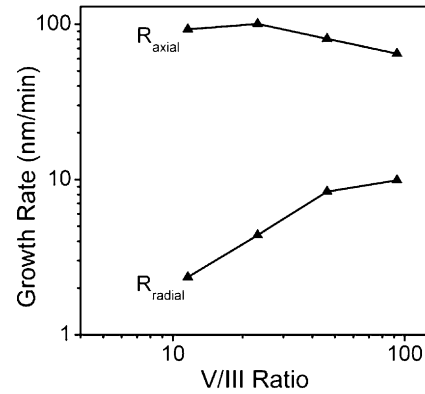


Fig. 15. Axial and radial growth rates of InAs nanowires for different V/III ratios. All samples were grown at 450 °C with a group III flow rate of III_0 . Axes are logarithmic.

havior of GaAs nanowires at high V/III ratios. InAs $(1\ 1\ 1)\text{B}$ surfaces, like GaAs $(1\ 1\ 1)\text{B}$ surfaces, form an As-trimer surface reconstruction under high As pressure [67]. This surface can decrease the $[1\ 1\ 1]\text{B}$ growth rate and also favor a growth direction other than $[1\ 1\ 1]\text{B}$. The short diffusion length at high V/III ratios also hinders axial nanowire growth while favoring planar growth on the substrate. This sets an upper limit on the V/III ratio that permits nanowire growth, which we denote the upper V/III limit.

The same overall trend, as shown in Fig. 15, was observed for all temperatures studied. However, with increasing temperature, the upper V/III limit and the peak of R_{axial} both shift to lower V/III ratios. This has also been noted in [63] and [66]. This can be explained considering the decomposition temperatures of TmIn and AsH_3 . TmIn decomposition is complete at 400 °C [58], whereas AsH_3 decomposition increases dramatically between 350 and 525 °C [68]. Therefore, as the nanowire growth temperature is raised, TmIn decomposition remains relatively steady, whereas AsH_3 decomposition increases. At higher temperatures, a given input V/III ratio will produce a higher effective As to In ratio. Therefore, as temperature is increased, the upper V/III limit and the peak of R_{axial} shift to lower input V/III ratios.

Fig. 16 compares InAs nanowires grown at different growth temperatures. The minimum temperature for straight $[1\ 1\ 1]\text{B}$ -oriented InAs nanowire growth was 400 °C. At the very low temperature of 375 °C, the Au nanoparticles have seeded the growth of irregular kinked nanostructures. This is similar to the irregular kinked GaAs nanowires grown at low temperatures, as discussed earlier. It is likely that the nanoparticle is solid at a growth temperature of 375 °C, and this solidification is responsible for irregular kinked growth, as proposed in the discussion of GaAs nanowire growth. By this reasoning, the nanoparticle is sufficiently melted at 400 °C and above to promote straight $[1\ 1\ 1]\text{B}$ -oriented InAs nanowire growth.

Interestingly, we found that the two-temperature procedure did not produce any advantages for InAs nanowire growth. Employing a high-temperature nucleation step did not achieve straight $[1\ 1\ 1]\text{B}$ -oriented nanowire growth at or below T_g of 375 °C.

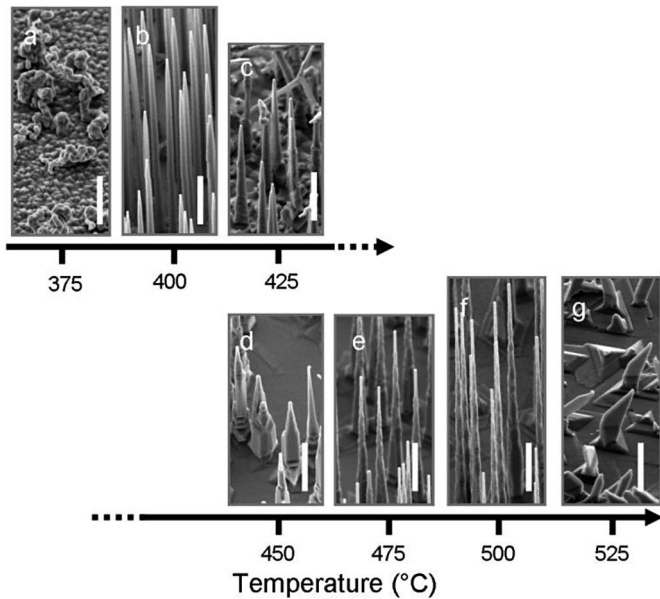


Fig. 16. FESEM images of InAs nanowires grown at different temperatures T_g , as indicated. The V/III ratio was 46 and the groups III and V flow rates were III_0 and V_0 , respectively, for all samples. Scale bars are $1 \mu\text{m}$. Samples are tilted at 40° .

This is reasonable because there is no pseudobinary Au–InAs tie line in the Au–In–As ternary phase diagram [44]. This means that, unlike GaAs substrates, InAs substrates readily react with the Au nanoparticle to form a Au–In alloy nanoparticle. Therefore, nanoparticle alloying and melting readily occur during pregrowth annealing. Therefore, a high-temperature nucleation step is unnecessary: the nanoparticle is already a liquid Au–In alloy. We infer that the minimum growth temperature of 400°C represents the minimum temperature for a liquid nanoparticle.

Binary phase diagrams show that the bulk Au–In eutectic temperature is 454.3°C [69], [70]. The solidification temperature we infer from our experiments, 375°C , is significantly lower. It is likely that Au–In nanoparticles do undergo melting–solidification hysteresis, similar to Au–Ga nanoparticles. This hysteresis was observed in [71]. The hysteresis effect is masked in the current InAs nanowire growth experiments because alloying takes place during pregrowth annealing, without requiring a nucleation step.

Fig. 17 plots InAs nanowire growth rate versus temperature. Apart from the observation of kinking at low temperatures, InAs nanowire growth exhibits a very different temperature dependency to GaAs nanowire growth. For GaAs nanowires, radial growth was kinetically limited throughout the range of temperatures examined (350 – 550°C). For InAs nanowires, radial growth was kinetically limited only at the lowest temperatures, between 400 and 425°C . In that range, R_{radial} increased with increasing temperature. As the temperature was raised above 450°C , radial growth moved into the mass transport limited regime, where it showed much less dependence on growth temperature. In the mass transport limited regime, radial growth depends more on the diffusion of adsorbed In species.

The diffusion length increases as temperature is raised [65]. This was evident in Fig. 12. A long diffusion length means that

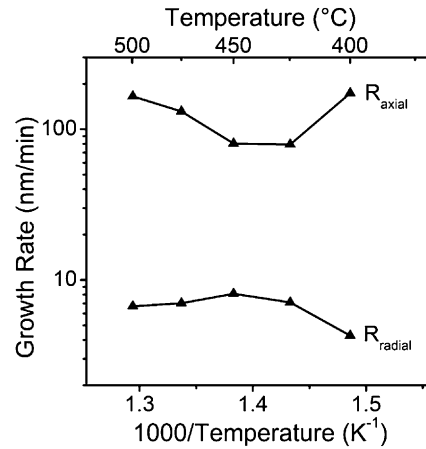


Fig. 17. Temperature dependence of axial and radial growth rates for InAs nanowires. Abscissa scale is logarithmic. The V/III ratio was 46 and the groups III and V flow rates were III_0 and V_0 , respectively, for all samples.

adsorbed In species are able to diffuse considerable distances to the energetically favorable position at the Au nanoparticle-capped nanowire tip. Consequently, as temperature is increased above 450°C , R_{axial} increases and R_{radial} decreases. This tapering dependence has been discussed in detail in [63].

In general, the axial growth rate shows the opposite trend to the radial growth rate. This is because radial growth competes significantly with axial growth for adsorbed diffusing In species. At 400°C , where R_{radial} is low, R_{axial} is high, and the same is observed at high temperatures.

At the highest temperature of 525°C , we witness an abrupt decrease in growth rate and the onset of nanowire kinking to $\langle 1\ 1\ 2 \rangle$ directions. As already discussed, higher temperatures give rise to a higher As to In ratio [66], which can inhibit $[1\ 1\ 1]\text{B}$ nanowire growth. This sets the upper temperature limit on InAs nanowire growth. In support of this explanation, the upper temperature limit shifts to higher temperatures as the input V/III ratio is lowered.

An interesting anomaly is observed at 425°C , at which nanowires are observed to kink. We believe that this occurs because at 425°C there is a local maximum in the ratio of available As to In species. One factor contributing to this local maximum is the relatively short diffusion length of In species at 425°C , which causes a shortage of In species at the nanowire tip. The second factor is that AsH_3 decomposition is relatively high at 425°C [68], which results in an abundance of As. This high As to In ratio could produce the As trimer reconstruction at the nanoparticle–nanowire interface, which interferes with $[1\ 1\ 1]\text{B}$ nanowire growth as already discussed. To test this reasoning, further nanowire samples were grown at 425°C with the same TMin flow, but with lower V/III ratios (12 and 23). The resulting nanowires were straight and $[1\ 1\ 1]\text{B}$ oriented. This confirms that a high effective As to In ratio is responsible for the kinking observed in Fig. 17(c).

Fig. 18 shows FESEM images of InAs nanowires grown with different absolute precursor flow rates. Fig. 19 plots the change in R_{axial} and R_{radial} with increasing absolute precursor flow rate. Three observations can be made. First, R_{axial} increased

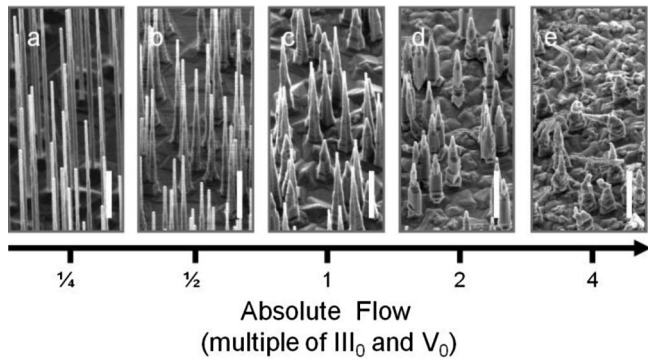


Fig. 18. FESEM images of InAs nanowires grown at the indicated absolute precursor flow rates. (a) $\frac{1}{4}$ III_0 and $\frac{1}{4}$ V_0 for $t = 120$ min, (b) $\frac{1}{2}$ III_0 and $\frac{1}{2}$ V_0 for $t = 60$ min, (c) III_0 and V_0 for $t = 30$ min, (d) 2III_0 and $2 V_0$ for $t = 15$ min, and (e) 4III_0 and $4 V_0$ for $t = 7.5$ min. All samples were grown at 450°C with a V/III ratio of 46. Scale bars are $1 \mu\text{m}$. Samples are tilted at 40° .

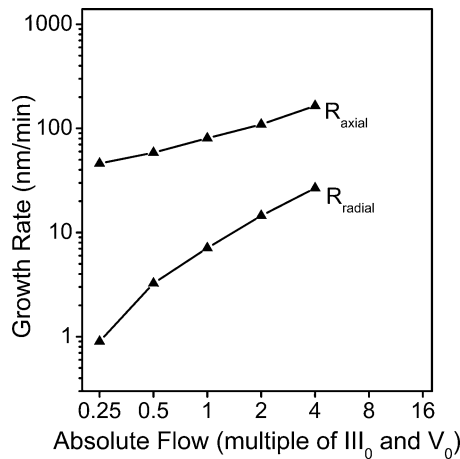


Fig. 19. Axial and radial growth rates of InAs nanowires for different group III flow rates. All samples were grown at 450°C with a V/III ratio of 46. Axes are logarithmic.

only marginally with increasing absolute precursor flow rate. Second, a strong increase in R_{radial} was observed. Finally, the substrate surface became increasingly irregular with increasing absolute flow rate.

These observations are very different to GaAs nanowire growth behavior. The differences between InAs and GaAs are clear when comparing Fig. 19 (for InAs nanowires) with Fig. 10 (for GaAs nanowires). These plots use the same scale so that comparison may be made. For InAs nanowires, R_{axial} has a weaker dependence and R_{radial} has a stronger dependence on absolute flow rate.

The three aforementioned observations point to a reduction in diffusion length with increasing growth rate. Indeed, it is well known that at low absolute precursor flow rates, there are fewer species deposited per unit time, so that the adsorbed species have more time to migrate and find energetically favorable sites to incorporate [65]. Consequently, at low precursor flow rates, In species can readily diffuse to the nanoparticle for incorporation into axial growth. At high precursor flow rates, on the other hand, In species have a much shorter diffusion length and are more likely to be incorporated close to the point of adsorption, either on the substrate or on the nanowire sidewalls. Thus, radial

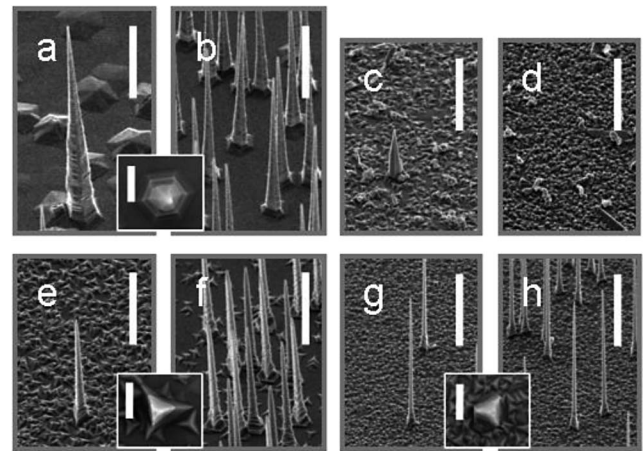


Fig. 20. FESEM images of nanowires grown by (a) and (b) single-temperature procedure with T_g of 450°C , (c) single-temperature procedure with T_g of 390°C , (d) single-temperature procedure with T_g of 375°C , (e) and (f) two-temperature procedure with T_g of 390°C , and (g) and (h) two-temperature procedure with T_g of 375°C . The insets were taken at 0° tilt and the scale bar is 500 nm . All other images were taken at 40° sample tilt and the scale bar is $2 \mu\text{m}$.

growth, tapering, and substrate growth significantly increase with absolute precursor flow rate. The axial growth rate, too, increases with absolute precursor flow rate, but only marginally due to the onset of significant radial and substrate growth, which consume diffusing In adatoms. At the highest flow rates [see Fig. 18(e)], the axial, substrate, and sidewall growth is highly irregular, presumably due to the short diffusion length.

InAs nanowire crystal structure exhibits the same trends as GaAs nanowires. As with GaAs nanowires, twin free ZB InAs nanowires were obtained by choosing a low growth temperature and high V/III ratio. Stacking fault-free WZ InAs nanowires were grown by using a high temperature and low V/III ratio [39].

C. InGaAs Nanowires

InGaAs nanowire growth is complicated by the different behavior of In and Ga species. Extensive investigations were carried out on InGaAs nanowires grown at 450°C [24]. InGaAs nanowires with high In composition showed a large density dependence, with higher R_{radial} and R_{axial} in regions of low nanowire density. Nanowires grown at 450°C feature significant tapering [see Fig. 20(a) and (b)], and are significantly taller and more tapered in regions of low nanowire density [see Fig. 20(a)] compared to regions of high nanowire density [see Fig. 20(b)].

This density dependence arises due to the long diffusion length of adsorbed In species on the GaAs (111)B substrate surface. The density dependence is analogous to the density dependence observed for InAs nanowires. The nanowire photoluminescence peak exhibited a red shift with decreasing nanowire density, due to the higher degree of In incorporation in more sparsely distributed InGaAs nanowires. In addition, EDS measurements found that these InGaAs nanowires exhibited a nonuniform composition: the In composition at the base was approximately three times higher than at the nanowire tip [24]. It is thought that the significant incorporation of diffusing In species into radial growth gives rise to an In-rich shell

structure around these tapered nanowires. Thus, unintentional In-rich radial growth is largely responsible for this compositional nonuniformity.

Device applications will require InGaAs nanowires with controllable, uniform composition, and uniform diameter. For this reason, it is important to minimize In-rich radial growth and tapering. Considering the preceding discussion of GaAs and InAs nanowire growth, we identify low growth temperature conditions as optimal for reducing radial growth.

Fig. 20 compares InGaAs nanowires grown with the single-temperature and two-temperature procedures at different T_g , with different densities. At T_g of 390 °C and below, (c) and (d), the single-temperature procedure produced nanowires with irregular morphologies: growth rarely initiated in the vertical (1 1 1)B direction, and kinking was common. This is analogous to the irregularity observed for GaAs and InAs nanowires grown below 400 °C.

In contrast, the two-temperature procedure allowed the growth of straight, vertical (1 1 1)B-oriented nanowires at temperatures at 390 °C and as low as 375 °C [see Fig. 20(g) and (h)]. Thus, low-temperature growth between 375 and 390 °C produces nanowires of poor morphologies, unless preceded by the high-temperature nucleation step using the two-temperature procedure.

At lower growth temperatures T_g of 390 and 375 °C [see Fig. 20(h)], there are several differences to the high temperature case of T_g of 450 °C [see Fig. 20(a) and (b)]. First, radial growth and tapering are reduced. A low growth temperature reduces tapering by two means: 1) it reduces the probability of overcoming the kinetic barrier for radial growth; and 2) it reduces the diffusion length [72], meaning a smaller flux of In and Ga species diffuse from the substrate and along nanowire sidewalls, to be incorporated into nanowire sidewalls. Secondly, the density dependence of nanowire height and tapering is suppressed. Density dependence is not apparent because at this low temperature, the diffusion length is so short that nanowires must be more closely spaced to compete for adsorbed species.

Thus, the two-temperature growth procedure produces straight, epitaxial (1 1 1)B-oriented InGaAs nanowires at significantly lower growth temperatures than previously achieved. By reducing the growth temperature, the In species diffusion length on the substrate is significantly reduced, and In-rich deposition on the sidewalls is limited.

Other parameters also exhibit potential for achieving high quality, compositionally uniform InGaAs nanowires. For example, low V/III ratios minimize radial growth for both GaAs and InAs nanowires. Therefore, a low V/III ratio is expected to produce minimally tapered InGaAs nanowires.

V. CONCLUSION

This paper enhances our understanding of GaAs and InAs nanowire growth, and also assists in plotting a course toward compositionally uniform, high-quality InGaAs nanowires. In particular, low growth temperatures present great advantages for the growth of high-quality InGaAs nanowires. These findings will greatly assist the development of future GaAs, InAs, and

InGaAs nanowire-based electronic and optoelectronic devices, and are expected to be more broadly relevant to the rational synthesis of other III-V nanowire materials.

ACKNOWLEDGMENT

The authors would like to thank their collaborators J. H. Kang, S. Paiman, and T. Burgess (Australian National University), J. Zou, M. Paladugu, X. Zhang, and Y. Guo (University of Queensland), H. Jackson, L. Smith, T. Hoang, L. Titova, M. Fickenscher, S. Perera, and M. Montazeri (University of Cincinnati), J. Yarrison-Rice (Miami University), and M. Johnston, L. Herz, and P. Parkinson (the University of Oxford). The Australian National Fabrication Facility, established under Australia's National Collaborative Research Infrastructure Strategy, provided access to the facilities used in this research.

REFERENCES

- [1] J. A. Czaban, D. A. Thompson, and R. R. LaPierre, "GaAs core-shell nanowires for photovoltaic applications," *Nano Lett.*, vol. 9, pp. 148–154, 2009.
- [2] C. J. Barrelet, A. B. Greytak, and C. M. Lieber, "Nanowire photonic circuit elements," *Nano Lett.*, vol. 4, pp. 1981–1985, 2004.
- [3] J. Wang, M. S. Gudiksen, X. Duan, Y. Cui, and C. M. Lieber, "Highly polarized photoluminescence and photodetection from single indium phosphide nanowires," *Science*, vol. 293, pp. 1455–1457, 2001.
- [4] H. Pettersson, J. Trägårdh, A. I. Persson, L. Landin, D. Hessman, and L. Samuelson, "Infrared photodetectors in heterostructure nanowires," *Nano Lett.*, vol. 6, pp. 229–232, 2006.
- [5] F. Qian, S. Gradedcak, Y. Li, C.-Y. Wen, and C. M. Lieber, "Core/multishell nanowire heterostructures as multicolor, high-efficiency light-emitting diodes," *Nano Lett.*, vol. 5, pp. 2287–2291, 2005.
- [6] E. D. Minot, F. Kelkensberg, M. van Kouwen, J. A. van Dam, L. P. Kouwenhoven, V. Zwiller, M. T. Borgstrom, O. Wunnicke, M. A. Verheijen, and E. P. A. M. Bakkers, "Single quantum dot nanowire LEDs," *Nano Lett.*, vol. 7, pp. 367–371, 2007.
- [7] A. H. Chin, S. Vaddiraju, A. V. Maslov, C. Z. Ning, M. K. Sunkara, and M. Meyyappan, "Near-infrared semiconductor subwavelength-wire lasers," *Appl. Phys. Lett.*, vol. 88, pp. 163115-1–163115-3, 2006.
- [8] B. Hua, J. Motohisa, Y. Kobayashi, S. Hara, and T. Fukui, "Single GaAs/GaAsP coaxial core-shell nanowire lasers," *Nano Lett.*, vol. 9, pp. 112–116, 2009.
- [9] M. T. Borgström, V. Zwiller, E. Muller, and A. Imamoglu, "Optically bright quantum dots in single nanowires," *Nano Lett.*, vol. 5, pp. 1439–1443, 2005.
- [10] M. T. Björk, B. J. Ohlsson, C. Thelander, A. I. Persson, K. Deppert, L. R. Wallenberg, and L. Samuelson, "Nanowire resonant tunneling diodes," *Appl. Phys. Lett.*, vol. 81, pp. 4458–4460, 2002.
- [11] C. Thelander, H. A. Nilsson, L. E. Jensen, and L. Samuelson, "Nanowire single-electron memory," *Nano Lett.*, vol. 5, pp. 635–638, 2005.
- [12] C. Thelander, T. Mårtensson, M. T. Björk, B. J. Ohlsson, M. W. Larsson, L. R. Wallenberg, and L. Samuelson, "Single-electron transistors in heterostructure nanowires," *Appl. Phys. Lett.*, vol. 83, pp. 2052–2054, 2003.
- [13] M. T. Björk, C. Thelander, A. E. Hansen, L. E. Jensen, M. W. Larsson, L. R. Wallenberg, and L. Samuelson, "Few-electron quantum dots in nanowires," *Nano Lett.*, vol. 4, pp. 1621–1625, 2004.
- [14] E. C. Heeres, E. P. A. M. Bakkers, A. L. Roest, M. Kaiser, T. H. Oosterkamp, and N. de Jonge, "Electron emission from individual indium arsenide semiconductor nanowires," *Nano Lett.*, vol. 7, pp. 536–540, 2007.
- [15] S. A. Dayeh, D. P. R. Aplin, X. Zhou, P. K. L. Yu, T. Yu Edward, and D. Wang, "High electron mobility InAs nanowire field-effect transistors," *Small*, vol. 3, pp. 326–332, 2007.
- [16] T. Bryllert, L.-E. Wernersson, T. Lowgren, and L. Samuelson, "Vertical wrap-gated nanowire transistors," *Nanotechnology*, vol. 17, pp. S227–S230, 2006.
- [17] H. T. Ng, J. Han, T. Yamada, P. Nguyen, Y. P. Chen, and M. Meyyappan, "Single crystal nanowire vertical surround-gate field-effect transistor," *Nano Lett.*, vol. 4, pp. 1247–1252, 2004.

- [18] E. Lind, A. I. Persson, L. Samuelson, and L.-E. Wernersson, "Improved subthreshold slope in an InAs nanowire heterostructure field-effect transistor," *Nano Lett.*, vol. 6, pp. 1842–1846, 2006.
- [19] C. J. Barrelet, J. Bao, M. Loncar, H.-G. Park, F. Capasso, and C. M. Lieber, "Hybrid single-nanowire photonic crystal and microresonator structures," *Nano Lett.*, vol. 6, pp. 11–15, 2006.
- [20] H.-G. Park, C. J. Barrelet, Y. Wu, B. Tian, F. Qian, and C. M. Lieber, "A wavelength-selective photonic-crystal waveguide coupled to a nanowire light source," *Nature Photon.*, vol. 2, pp. 622–626, 2008.
- [21] Y. Cui, Q. Wei, H. Park, and C. M. Lieber, "Nanowire nanosensors for highly sensitive and selective detection of biological and chemical species," *Science*, vol. 293, pp. 1289–1292, 2001.
- [22] A. G. Milnes and A. Y. Polyakov, "Indium arsenide: A semiconductor for high speed and electro-optical devices," *Mater. Sci. Eng. B*, vol. 18, pp. 237–259, 1993.
- [23] C. A. Mead and W. G. Spitzer, "Fermi level position at semiconductor surfaces," *Phys. Rev. Lett.*, vol. 10, pp. 471–472, 1963.
- [24] Y. Kim, H. J. Joyce, Q. Gao, H. H. Tan, C. Jagadish, M. Paladugu, J. Zou, and A. A. Suvorova, "Influence of nanowire density on the shape and optical properties of ternary InGaAs nanowires," *Nano Lett.*, vol. 6, pp. 599–604, 2006.
- [25] F. Jabeen, S. Rubini, and F. Martelli, "Growth of III-V semiconductor nanowires by molecular beam epitaxy," *Microelectron. J.*, vol. 40, pp. 442–445, 2009.
- [26] T. Sato, J. Motohisa, J. Noborisaka, S. Hara, and T. Fukui, "Growth of InGaAs nanowires by selective-area metalorganic vapor phase epitaxy," *J. Crystal Growth*, vol. 310, pp. 2359–2364, 2008.
- [27] I. Regolin, V. Khorenko, W. Prost, F.-J. Tegude, D. Sudfeld, J. Kastner, and G. Dumpich, "Composition control in metal-organic vapor-phase epitaxy grown InGaAs nanowires," *J. Appl. Phys.*, vol. 100, pp. 074321–1–074321-5, 2006.
- [28] J. Bauer, V. Gottschalch, H. Paetzelt, and G. Wagner, "VLS growth of GaAs/(InGa)As/GaAs axial double-heterostructure nanowires by MOVPE," *J. Crystal Growth*, vol. 310, pp. 5106–5110, 2008.
- [29] J. Noborisaka, T. Sato, J. Motohisa, S. Hara, K. Tomioka, and T. Fukui, "Electrical characterizations of InGaAs nanowire-top-gate field-effect transistors by selective-area metal organic vapor phase epitaxy," *Jpn. J. Appl. Phys.*, vol. 46, pp. 7562–7568, 2007.
- [30] K. Hiruma, M. Yazawa, K. Haraguchi, K. Ogawa, T. Katsuyama, M. Koguchi, and H. Kakibayashi, "GaAs freestanding quantum-size wires," *J. Appl. Phys.*, vol. 74, pp. 3162–3171, 1993.
- [31] K. A. Dick, K. Deppert, L. S. Karlsson, L. R. Wallenberg, L. Samuelson, and W. Seifert, "A new understanding of Au-assisted growth of III-V semiconductor nanowires," *Adv. Funct. Mater.*, vol. 15, pp. 1603–1610, 2005.
- [32] D. J. Wolford, G. D. Gilliland, T. F. Kuech, J. F. Klem, H. P. Hjalmarson, J. A. Bradley, C. F. Tsang, and J. Martinsen, "Comparison of transport, recombination, and interfacial quality in molecular beam epitaxy and organometallic vapor-phase epitaxy GaAs/Al_xGa_{1-x}As structures," *Appl. Phys. Lett.*, vol. 64, pp. 1416–1418, 1994.
- [33] R. L. Moon, "MOVPE: Is there any other technology for optoelectronics?," *J. Crystal Growth*, vol. 170, pp. 1–10, 1997.
- [34] M. Behet, R. Hövel, A. Kohl, A. M. Küsters, B. Opitz, and K. Heime, "MOVPE growth of III-V compounds for optoelectronic and electronic applications," *Microelectron. J.*, vol. 27, pp. 297–334, 1996.
- [35] G. B. Stringfellow, *Organometallic Vapor-Phase Epitaxy: Theory and Practice*, 2nd ed. San Diego, CA: Academic Press, 1999.
- [36] H. J. Joyce, Q. Gao, H. H. Tan, C. Jagadish, Y. Kim, X. Zhang, Y. Guo, and J. Zou, "Twin-free uniform epitaxial GaAs nanowires grown by a two-temperature process," *Nano Lett.*, vol. 7, pp. 921–926, 2007.
- [37] J. Zou, M. Paladugu, H. Wang, G. J. Auchterlonie, Y. Guo, Y. Kim, Q. Gao, H. J. Joyce, H. H. Tan, and C. Jagadish, "Growth mechanism of truncated triangular III-V nanowires," *Small*, vol. 3, pp. 389–393, 2007.
- [38] M. A. Verheijen, R. E. Algra, M. T. Borgstrom, G. Immink, E. Sourty, W. J. P. van Enckevort, E. Vlieg, and E. P. A. M. Bakkers, "Three-dimensional morphology of GaP-GaAs nanowires revealed by transmission electron microscopy tomography," *Nano Lett.*, vol. 7, pp. 3051–3055, 2007.
- [39] H. J. Joyce, J. Wong-Leung, Q. Gao, H. H. Tan, and C. Jagadish, "Phase perfection in zinc blende and wurtzite III-V nanowires using basic growth parameters," *Nano Lett.*, vol. 10, pp. 908–915, 2010.
- [40] S. A. Dayeh, E. T. Yu, and D. Wang, "Surface diffusion and substrate-nanowire adatom exchange in InAs nanowire growth," *Nano Lett.*, vol. 9, pp. 1967–1972, 2009.
- [41] H. Okamoto and T. Massalski, "The As-Au (arsenic-gold) system," *J. Phase Equil.*, vol. 5, pp. 56–59, 1984.
- [42] S. Kodambaka, J. Tersoff, M. C. Reuter, and F. M. Ross, "Germanium nanowire growth below the eutectic temperature," *Science*, vol. 316, pp. 729–732, 2007.
- [43] M. Tchernycheva, J. C. Harmand, G. Patriarche, L. Travers, and G. E. Cirilin, "Temperature conditions for GaAs nanowire formation by Au-assisted molecular beam epitaxy," *Nanotechnology*, vol. 17, pp. 4025–4030, 2006.
- [44] C. T. Tsai and R. S. Williams, "Solid phase equilibria in the Au-Ga-As, Au-Ga-Sb, Au-In-As, and Au-In-Sb ternaries," *J. Mater. Res.*, vol. 1, pp. 352–360, 1986.
- [45] D. H. Reep and S. K. Ghandhi, "Deposition of GaAs epitaxial layers by organometallic CVD," *J. Electrochem. Soc.*, vol. 130, pp. 675–680, 1983.
- [46] M. T. Borgström, G. Immink, B. Ketelaars, R. E. Algra, and E. P. A. M. Bakkers, "Synergetic nanowire growth," *Nature Nano.*, vol. 2, pp. 541–544, 2007.
- [47] S. A. Dayeh, E. T. Yu, and D. Wang, "Growth of InAs nanowires on SiO₂ substrates: Nucleation, evolution, and the role of Au nanoparticles," *J. Phys. Chem. C*, vol. 111, pp. 13331–13336, 2007.
- [48] W. Seifert, M. Borgström, K. Deppert, K. A. Dick, J. Johansson, M. W. Larsson, T. Mårtensson, N. Sköld, C. P. T. Svensson, B. A. Wacaser, L. R. Wallenberg, and L. Samuelson, "Growth of one-dimensional nanostructures in MOVPE," *J. Crystal Growth*, vol. 272, pp. 211–220, 2004.
- [49] M. A. Verheijen, G. Immink, T. de Smet, M. T. Borgström, and E. P. A. M. Bakkers, "Growth kinetics of heterostructured GaP-GaAs nanowires," *J. Amer. Chem. Soc.*, vol. 128, pp. 1353–1359, 2006.
- [50] C. Soci, X.-Y. Bao, D. P. R. Aplin, and D. Wang, "A systematic study on the growth of GaAs nanowires by metal-organic chemical vapor deposition," *Nano Lett.*, vol. 8, pp. 4275–4282, 2008.
- [51] D. H. Reep and S. K. Ghandhi, "Electrical properties of organometallic chemical vapor deposited GaAs epitaxial layers," *J. Electrochem. Soc.*, vol. 131, pp. 2697–2702, 1984.
- [52] K. Ikejiri, J. Noborisaka, S. Hara, J. Motohisa, and T. Fukui, "Mechanism of catalyst-free growth of GaAs nanowires by selective area MOVPE," *J. Crystal Growth*, vol. 298, pp. 616–619, 2007.
- [53] H. J. Joyce, Q. Gao, H. H. Tan, C. Jagadish, Y. Kim, M. A. Fickenscher, S. Perera, T. B. Hoang, L. M. Smith, H. E. Jackson, J. M. Yarrison-Rice, X. Zhang, and J. Zou, "High purity GaAs nanowires free of planar defects: Growth and characterization," *Adv. Funct. Mater.*, vol. 18, pp. 3794–3800, 2008.
- [54] L. V. Titova, T. B. Hoang, H. E. Jackson, L. M. Smith, J. M. Yarrison-Rice, Y. Kim, H. J. Joyce, H. H. Tan, and C. Jagadish, "Temperature dependence of photoluminescence from single core-shell GaAs-AlGaAs nanowires," *Appl. Phys. Lett.*, vol. 89, pp. 173126-1–173126-3, 2006.
- [55] S. Perera, M. A. Fickenscher, H. E. Jackson, L. M. Smith, J. M. Yarrison-Rice, H. J. Joyce, Q. Gao, H. H. Tan, C. Jagadish, X. Zhang, and J. Zou, "Nearly intrinsic exciton lifetimes in single twin-free GaAs/AlGaAs core-shell nanowire heterostructures," *Appl. Phys. Lett.*, vol. 93, pp. 053110-1–053110-3, 2008.
- [56] H. J. Joyce, Q. Gao, H. H. Tan, C. Jagadish, Y. Kim, M. A. Fickenscher, S. Perera, T. B. Hoang, L. M. Smith, H. E. Jackson, J. M. Yarrison-Rice, X. Zhang, and J. Zou, "Unexpected benefits of rapid growth rate for III-V nanowires," *Nano Lett.*, vol. 9, pp. 695–701, 2009.
- [57] P. Parkinson, H. J. Joyce, Q. Gao, H. H. Tan, X. Zhang, J. Zou, C. Jagadish, L. M. Herz, and M. B. Johnston, "Carrier lifetime and mobility enhancement in nearly defect-free core-shell nanowires measured using time-resolved terahertz spectroscopy," *Nano Lett.*, vol. 9, pp. 3349–3353, 2009.
- [58] N. I. Buchan, C. A. Larsen, and G. B. Stringfellow, "Mass spectrometric studies of trimethylindium pyrolysis," *J. Crystal Growth*, vol. 92, pp. 591–604, 1988.
- [59] C. A. Larsen, N. I. Buchan, S. H. Li, and G. B. Stringfellow, "Decomposition mechanisms of trimethylgallium," *J. Crystal Growth*, vol. 102, pp. 103–116, 1990.
- [60] C. A. Larsen, S. H. Li, N. I. Buchan, G. B. Stringfellow, and D. W. Brown, "Kinetics of the reaction between trimethylgallium and arsine," *J. Crystal Growth*, vol. 102, pp. 126–136, 1990.
- [61] J. E. Butler, N. Bottka, R. S. Sillmon, and D. K. Gaskill, "In situ, real-time diagnostics of OMVPE using IR-diode laser spectroscopy," *J. Crystal Growth*, vol. 77, pp. 163–171, 1986.
- [62] K. Ma, Z. Fang, R. Cohen, and G. B. Stringfellow, "Ultra-low temperature OMVPE of InAs and InAsBi," *J. Electron. Mater.*, vol. 21, pp. 143–148, 1992.
- [63] K. A. Dick, K. Deppert, L. Samuelson, and W. Seifert, "Optimization of Au-assisted InAs nanowires grown by MOVPE," *J. Crystal Growth*, vol. 297, pp. 326–333, 2006.
- [64] J. H. Pugh and R. S. Williams, "Entropy-driven loss of gas phase group V species from gold/III-V compound semiconductor systems," *J. Mater. Res.*, vol. 1, pp. 343–351, 1986.

- [65] Z. H. Zhang, G. W. Pickrell, K. L. Chang, H. C. Lin, K. C. Hsieh, and K. Y. Cheng, "Surface morphology control of InAs nanostructures grown on InGaAs/InP," *Appl. Phys. Lett.*, vol. 82, pp. 4555–4557, 2003.
- [66] S. A. Dayeh, E. T. Yu, and D. Wang, "III-V nanowire growth mechanism: V/III ratio and temperature effects," *Nano Lett.*, vol. 7, pp. 2486–2490, 2007.
- [67] A. Taguchi, "First-principles investigations of surface reconstructions of an InAs(111)B surface," *J. Crystal Growth*, vol. 278, pp. 468–472, 2005.
- [68] R. Lückcrath, P. Tommack, A. Hertling, H. J. Koss, P. Balk, K. F. Jensen, and W. Richter, "CARS in situ diagnostics in MOVPE: The thermal decomposition of AsH₃ and PH₃," *J. Crystal Growth*, vol. 93, pp. 151–158, 1988.
- [69] S. E. R. Hiscocks and W. Hume-Rothery, "The equilibrium diagram of the system gold-indium," *Proc. R. Soc. London A*, vol. 282, pp. 318–330, 1964.
- [70] H. Okamoto, "Au-In (gold-indium)," *J. Phase Equil.*, vol. 25, pp. 197–198, 2004.
- [71] M. Tchernycheva, L. Travers, G. Patriarche, F. Glas, J.-C. Harmand, G. E. Cirlin, and V. G. Dubrovskii, "Au-assisted molecular beam epitaxy of InAs nanowires: Growth and theoretical analysis," *J. Appl. Phys.*, vol. 102, pp. 094313-1–094313-8, 2007.
- [72] J. Johansson, C. P. T. Svensson, T. Mårtensson, L. Samuelson, and W. Seifert, "Mass transport model for semiconductor nanowire growth," *J. Phys. Chem. B*, vol. 109, pp. 13567–13571, 2005.



Hannah J. Joyce (S'05) was born in Perth, Western Australia. She received the B.Sc. and B.E. (Hons.) degrees, majoring in pharmacology and electrical and electronic engineering, from the University of Western Australia, Perth, Australia, in 2005, and the Ph.D. degree from the Australian National University (ANU), Canberra, Australia, in 2009. She was a Postdoctoral Fellow at the ANU until May 2010.

At ANU, she investigated the growth and characterization of III-V semiconductor nanowires for optoelectronic device applications. While working toward the Ph.D. degree, she authored and co-authored over 20 journal publications. Since May 2010, she has been a Postdoctoral Fellow at the University of Oxford, Oxford, U.K., where she is investigating terahertz spectroscopy to characterize III-V semiconductor nanowires.



Qiang Gao (S'02–M'05) received the Bachelor's and M.S. degrees in materials engineering from Northeastern University, Shenyang, China, in 1994 and 1997, respectively, and the Ph.D. degree in electronics engineering from the Australian National University (ANU), Canberra, Australia, in 2004.

In 2006, he was a Postdoctoral Fellow and was awarded the Australian Research Council (ARC) Postdoctoral Fellowship, in the Department of Electronic Materials Engineering, ANU, where he was engaged in research on metal-organic chemical vapor deposition growth of III-V compound semiconductor nanostructures including quantum dots and nanowires, and fabrication of optoelectronic devices. In 2010, he was awarded the ARC Research Fellowship for five years. He is currently a Research Fellow in the Department of Electronic Materials Engineering, ANU, and is engaged in nanowire research. He is the author or coauthor of more than 40 journal papers.



Jennifer Wong-Leung received the B.Sc. (Hons.) degree in physics from the University of Bristol, Bristol, U.K., in 1991, and the Ph.D. degree on gettering of metals in silicon to defects induced by ion implantation degree from the Australian National University (ANU), Canberra, Australia, in 1997.

She is currently a Fellow in the Department of Electronic Materials Engineering, Research School of Physics and Engineering, ANU. She is the author or coauthor of more than 60 journal publications. Her research interests include transmission electron microscopy of defects in semiconductors, quantum dots and nanowires, ion implantation, and electrical characterization of defects in ion-implanted semiconductors including wide bandgap semiconductors.

Yong Kim was born in Seoul, Korea, 1961. He received the B.S. degree from Seoul National University, Seoul, Korea, in 1983, and the M.S. and Ph.D. degrees from the Korea Advanced Institute of Science and Technology, Daejeon, Korea, in 1985 and 1991, respectively, all in physics.

From 1985 to 1999, he was a Research Scientist at the Korea Institute of Science and Technology. From 1991 to 1999, he was a Senior Research Scientist at the same institute, where he was engaged in research on the epitaxial growth of III-V compound semiconductor structure by metal-organic chemical vapor deposition. From 1995 to 1996, he was an Australian Research Council International Fellow at the Australian National University, Canberra, Australia, where he joined the research team led by Prof. Chennupati Jagadish and studied the growth of quantum wires on nonplanar substrates. In 1999, he joined Dong-A University, Busan, Korea, where he is currently a Professor in the Department of Physics. From 2005 to 2006, he was a member of Academic Staff at the Australian National University, Canberra, Australia, where he was engaged in III-V nanowire growth by metal-organic chemical vapor deposition. He is the author or coauthor of more than 150 research papers published in the international journals. His current research interests include the growth and characterization of semiconductor nanowires, nanobelts and nanosheets by chemical vapor deposition, molecular beam deposition, and physical vapor transport.



H. Hoe Tan (SM'03) was born in Penang, Malaysia. He received the B.E. (Hons.) degree in electrical engineering from the University of Melbourne, Victoria, Australia, in 1992, and the Ph.D. degree from the Australian National University (ANU), Canberra, Australia. His Ph.D. thesis focused on "Ion beam effects in GaAs–AlGaAs materials and devices."

In 1992, he was a Quality Assurance Engineer with Siemens (currently known as Osram) in Penang, Malaysia. He is currently an Associate Professor in the Department of Electronic Materials Engineering, Research School of Physics and Engineering, ANU. He is the author or coauthor of over published 220 journal papers, 1 review article, a book chapter, and has presented over 20 invited talks at international conferences. He is also a co-inventor in four US patents related to laser diodes and infrared photodetectors. His research interests include epitaxial growth of low-dimensional compound semiconductors, ion-implantation processing of compound semiconductors for optoelectronic device applications, and optoelectronic devices.



Chennupati Jagadish (S'84–M'86–M'89–SM'92–F'02) received the Ph.D. degree in physics from Delhi University, in 1986.

From 1988 to 1990, he was a Postdoctoral Fellow at Queen's University, Kingston, ON. In 1990, he joined the Australian National University (ANU), Canberra, Australia, where he has established a major research program in compound semiconductor optoelectronics and nanotechnology. He is currently an Australian Laureate Fellow, Distinguished Professor, and Head of the Semiconductor Optoelectronics and Nanotechnology Group, ANU. He is the author or coauthor of more than 400 published journal papers and holds 5 US patents. He has coauthored a book on semiconductor transparent thin films, coedited a book on zinc oxide: *Bulk, Thin Films and Nanostructures*, edited 12 conference proceedings, and guest edited 5 special issues of journals. His research interests include compound semiconductors, lasers, photodetectors, solar cells, photonic integrated circuits, quantum dots, nanowires, THz photonics, photonic crystals, metamaterials, and plasmonics. He is an Editor of *Progress in Quantum Electronics* and is on the editorial boards of 12 other journals.

Prof. Jagadish is an Associate Editor of the IEEE ELECTRON DEVICE LETTERS. He is the recipient of the IEEE Third Millennium Medal in 2000, the Peter Baume Award from the ANU, the 2010 Quantum Devices Award, and the 2010 IEEE Photonic Society Distinguished Service Award.